

Numerical Study of Heat Transfer in Scissors-shaped Roofs

Ola KAMIYO

Department of Mechanical Engineering, University of Lagos, Lagos, Nigeria
okamiyo@unilag.edu.ng

Corresponding Author: okamiyo@unilag.edu.ng, +2348157992038

Date Submitted: 26/01/2021

Date Accepted: 10/03/2021

Date Published: 30/06/2021

Abstract: Thermal characteristics of the attic space are known to influence the thermal comfort and energy efficiency within the space directly below it. Among past studies reported, very few have been on complex-shaped rooftops which are becoming common. This study therefore focused on steady-state, two-dimensional laminar natural convection heat transfer of air in long, scissors-shaped attic of selected pitch angles heated through the ceiling. A finite volume numerical simulation approach is adopted. Results obtained show that the streamlines depict multiple, recirculating, counter-rotating cells symmetrically positioned within the enclosures. The intensity and size of the vortices decrease from the middle of an enclosure towards the bottom corners and as the enclosure pitch increases. The pattern of the variation synchronizes with the detachment of the hot plumes from and the attachment of the cold jets to the hot wall. Heat transfer rate is high at locations where cold jets drop on the hot wall but low where hot air separates from the hot wall. The mean Nusselt number for the hot ceiling decreases with the pitch angle. Therefore, in temperate region, to minimize the rate of heat loss from a heated occupied space below into the attic above through the ceiling, the pitch angle of the roof should be relatively high. For low-pitch roof buildings in such location, the ceiling insulation should be of appropriate quality and thickness.

Keywords: heat transfer, heated below, natural convection, pitch angle, pitch roof, scissors-shaped.

1. INTRODUCTION

Studies on the airflow and heat characteristics within enclosed surfaces have attracted attention over the years due to their relevance in the designs of rooftops, ventilation and air-conditioning systems, solar equipment and cooling of electronic boards. After the foundational studies carried out by Flack [1] on the experiment and simulation of pitched rooftop and Akinsete and Coleman [2] on the simulation of triangular rooftop models, heat and airflow distributions within the attic and heat flow across the ceiling have been the focus of research. Advances in numerical methods employed in computational fluid dynamic (CFD) packages have led to near-accurate predictions of natural convective heat transfer in enclosures. Extensive reviews of extant literature carried out by Kamiyo *et al.* [3] and Das *et al.* [4] on regular triangular and a few complex roofs discussed the effects of air properties and roof configurations on the flow pattern and heat distribution.

In the past decade, many studies on heat transfer within attics have been reported. In recent times, convective and radiative heat transfer analysis of fluid flow inside a regular triangular cavity was studied by Moftakhari *et al.* [5] using natural element numerical method. Basak *et al.* [6] used the Bejan's heatline approach to investigate natural convection in porous right-angled triangular enclosures with a concave and convex hypotenuse. Thermal mixing is found higher in convex case than in the concave case for all parameters considered. Haghghi *et al.* [7] reported improvement in the thermal comfort in a building with vented vaulted roof. Using roof-integrated, radiative air-cooling system, Zhao *et al.* [8] were able to reduce the attic temperature of a building. Complex roofs studied so far include those by Das and Morsi [9] -dome, Mahmoudi *et al.* [10] -inclined triangular cavity, Kamiyo *et al.* [11] -asymmetric triangular cavity, Saha and Gu [12] -baffled triangular enclosure, Sieres *et al.* [13] -vertical upright-angled triangular cavity, Amrani *et al.* [14] -gable roof, Cui *et al.* [15] -sectioned-triangular prismatic enclosure. Elnokaly *et al.* [16] -vaulted roof, Mehryan *et al.* [17] -trapezoidal and square cavities and Kamiyo [18] -raised ceiling attic. A number of other complex roofs have been investigated; nonetheless, there are still some other common ones that have not been studied sufficiently. Therefore, this study uses a finite-volume CFD package to investigate steady, natural convective airflow and heat transfer within the attic of a scissor-shaped roof heated through the ceiling.

2. METHODOLOGY

In this study, a long, horizontal attic space with scissors-shaped cross-section extending more than double its width, as shown in Figure 1, is considered. Penot and N'Dame [19] confirmed that the flowfield and heat transfer in enclosures with such geometry could be regarded as two-dimensional.

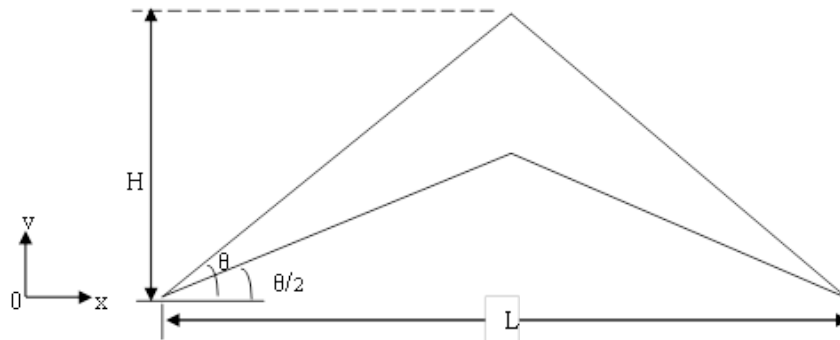


Figure 1: Physical model

The attic space is filled with air and there is no internal generation of heat. Since the size of a roof depends on the building dimensions, the physical domain, which matches the computational domain, with the boundary conditions are normalized. The dimensionless forms of the governing equations for steady laminar flow subject to Boussinesq approximation [20, 21] are expressed as:

Conservation of Mass:

$$\frac{\partial U}{\partial X} + \frac{\partial V}{\partial Y} = 0 \quad (1)$$

Conservation of Momentum:

X-momentum:

$$U \frac{\partial U}{\partial X} + V \frac{\partial U}{\partial Y} = -\frac{\partial P}{\partial X} + Pr \left(\frac{\partial^2 U}{\partial X^2} + \frac{\partial^2 U}{\partial Y^2} \right) \quad (2)$$

Y-momentum:

$$U \frac{\partial V}{\partial X} + V \frac{\partial V}{\partial Y} = -\frac{\partial P}{\partial Y} + Pr \left(\frac{\partial^2 V}{\partial X^2} + \frac{\partial^2 V}{\partial Y^2} \right) + RaPr\theta \quad (3)$$

Conservation of Energy

$$U \frac{\partial \theta}{\partial X} + V \frac{\partial \theta}{\partial Y} = \left(\frac{\partial^2 \theta}{\partial X^2} + \frac{\partial^2 \theta}{\partial Y^2} \right) \quad (4)$$

where $X = \frac{x}{L}$, $Y = \frac{y}{L}$, $V = \frac{vL}{\alpha}$, $U = \frac{uL}{\alpha}$, $\theta = \frac{T-T_C}{T_H-T_C}$, $P = \frac{pL^2}{\rho\alpha^2}$, $Pr = \frac{\nu}{\alpha}$, and

$$Ra = \frac{g\beta(T_H-T_C)H^3}{\alpha\nu}$$

with the following boundary conditions:

Hot lower wall, $U = V = 0$; $\theta = 1$.

Cold upper wall, $U = V = 0$; $\theta = 0$.

That means no slip condition applies at all the walls.

Four angles within standard range for pitch roofs are arbitrarily selected; the details are as stated in Table 1.

Table 1: Parametric details of the enclosures

Pitch Angle (ϕ)	14°	18°	30°	45°
Aspect Ratio (AR)	0.25	0.325	0.58	1.00
Rayleigh Number (Ra)	3×10^5	7×10^5	4×10^6	2×10^7

Unstructured very fine mesh was generated for the computational domain with attention paid to areas in proximity to the walls and corners to properly capture changes within the boundary layers. The grid for the 30° pitch is shown in Figure 2. Using a finite-volume based ANSYS FLUENT® (Version 18) solver, the coupled, nonlinear governing partial differential equations (1) – (4) were solved numerically. The SIMPLE algorithm was used to resolve the pressure-velocity

coupling. Pressure interpolation was handled using the PRESTO scheme. QUICK scheme was used to spatially discretize the momentum and energy equations. To ensure proper convergence, 10^{-5} was fixed as convergence criterion for the continuity and 10^{-7} for the momentum and energy equations. The governing equations were solved iteratively to obtain a converged solution for each enclosure.



Figure 2: Computational grid for the 30° pitch enclosure

Many numerical runs were conducted for an enclosure at grids with different number of elements to test grid independence of the results. The maximum value of the velocity magnitude for each grid is shown in Table 2. The results show that a mesh size of 64,000 elements was sufficient to produce grid independence in the 18° enclosure.

Table 2: Grid independence test for the 18° roof pitch enclosure

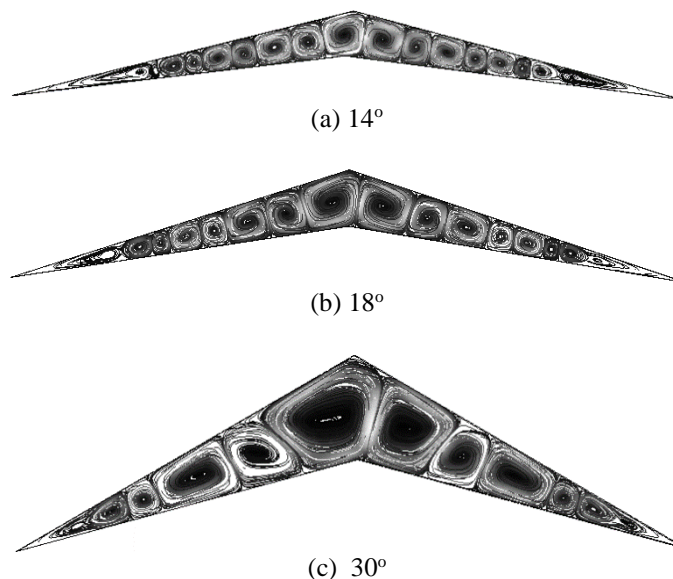
Number of elements	56,424	64,291	70,673
U_{max} (m/s)	0.04	0.05	0.05

3. RESULTS AND DISCUSSION

The results obtained in the simulation are shown in Figures 3-11 in the form of streamlines, contour plots of the magnitude of air velocity and isotherms, graphical plots of the variations of the air velocity and temperature across some selected sections, graphical plots of the local Nusselt number variation along the hot ceiling of the 45° enclosure and of the changes in the mean Nusselt number of the hot wall with enclosure pitch angle.

3.1 Streamlines

In Figure 3, the streamlines for different roof pitches are presented. The convection system shows streams of hot, buoyancy-driven air, in form of plumes, move up from the hot lower wall, smash on the cold upper wall and bifurcate in right and left directions. Losing a major part of the heat content, the air detach as cold dense jets, flows downward to be reheated by the hot lower wall to regain momentum and recur the convection process. As a result, at steady state, there forms a multiple of revolving cells, arranged quasi-symmetrically. The bifurcation of the plumes at the cold wall makes the cell on its right to rotate clockwise and that on the left to rotate anticlockwise thereby forming a system of counter-rotating adjacent cells.



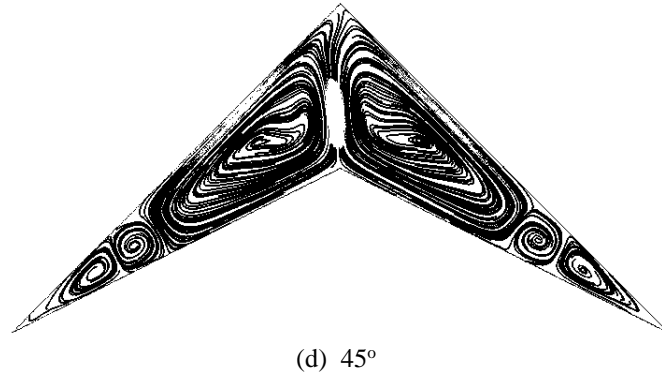
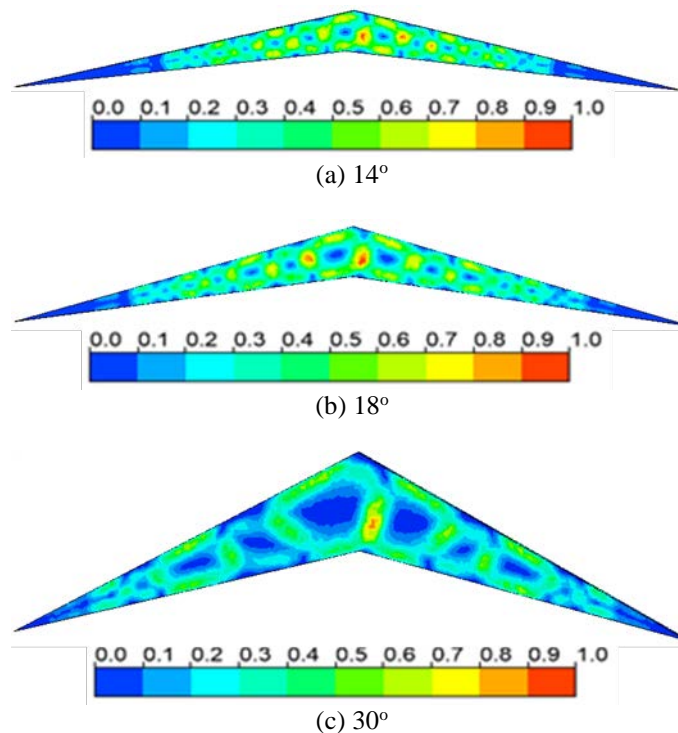


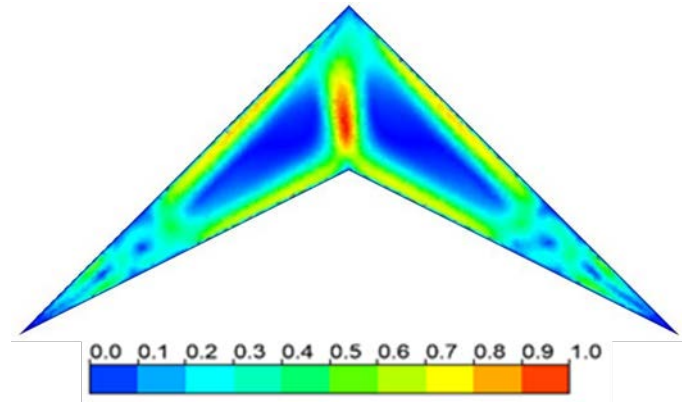
Figure 3: Streamlines for different pitch angles

In the 14° enclosure, there are sixteen recirculating vortices. The size of the vortices and their intensities are observed to reduce from the midsection to the lower corners. The number of the cells remains the same in the 18° enclosure but the sizes marginally increase. This is because the few degrees increase in the pitch angle could not cause merging or bifurcation of cells. However, in the 30° enclosure, the size of the cells has become bigger while the number has reduced to ten as some adjacent cells in the 14° enclosure appeared to have merged. In the 45° enclosure, with the pitch angle increased about three times, the number of cells is found to have reduced to about a third of that in the 14° enclosure. The multiple counter-rotating vortices obtained in this result is similar to that of Holtzman *et al.* [22] who reported multicellular airflow pattern in their flow visualization experiments in isosceles triangular enclosures heated from the base wall.

3.2 Velocity Distribution

Distribution of air velocity in each of the enclosures is presented in Figure 4. In all the enclosures, values of velocity are relatively higher at locations where adjacent cells rub on each other or on the walls. The velocity is highest around the cells at the midsection and reduces towards the lower corners. As the roof pitch increases, average velocity across the attic reduces because the heating effect of the lower wall was also reducing.





(d) 45°

Figure 4: Air velocity distribution for different enclosures

Characteristically, the value of the velocity across a cell reduces from the outer circumference towards the core; depending on the relative intensity of the vortex. At the lower corners, conduction dominates. Therefore, there is no movement of air there. This stagnant area reduces with increase in the pitch angle.

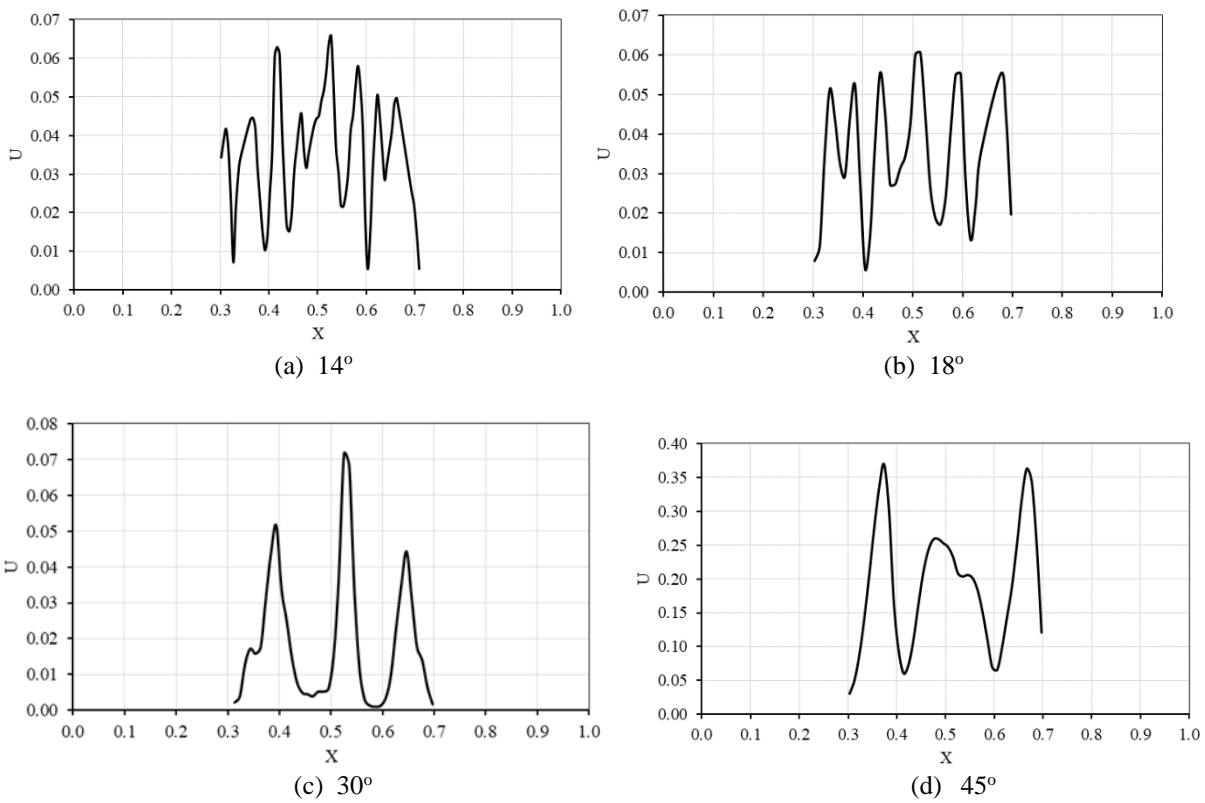


Figure 5: Air velocity across $Y = 0.6H$ within different enclosures

Figure 5 shows the variation of the values of the velocity at a cross-section slightly above the midheight ($Y = 0.6H$) for each enclosure. The sequence of the variation signifies the parts of the cells within the enclosure that fall on the cross-sectional line. The peaks correspond to the parts of the plumes and jets while the troughs fall within the inner parts of the cells. In all the enclosures, the peak at the middle is for a plume. Hence, the peaks on either side of it correspond to that of jets followed by another plume and another jet in that order. Thus, the gap between adjacent peaks indicates a chord of a cell. The high number of peaks in Figure 5(a) is due to the number of plumes and jets in the 14° enclosure (Figure 7(a)). From the plot, it could be possible to predict the size of a cell and its strength at a point in the attic with a particular pitch angle.

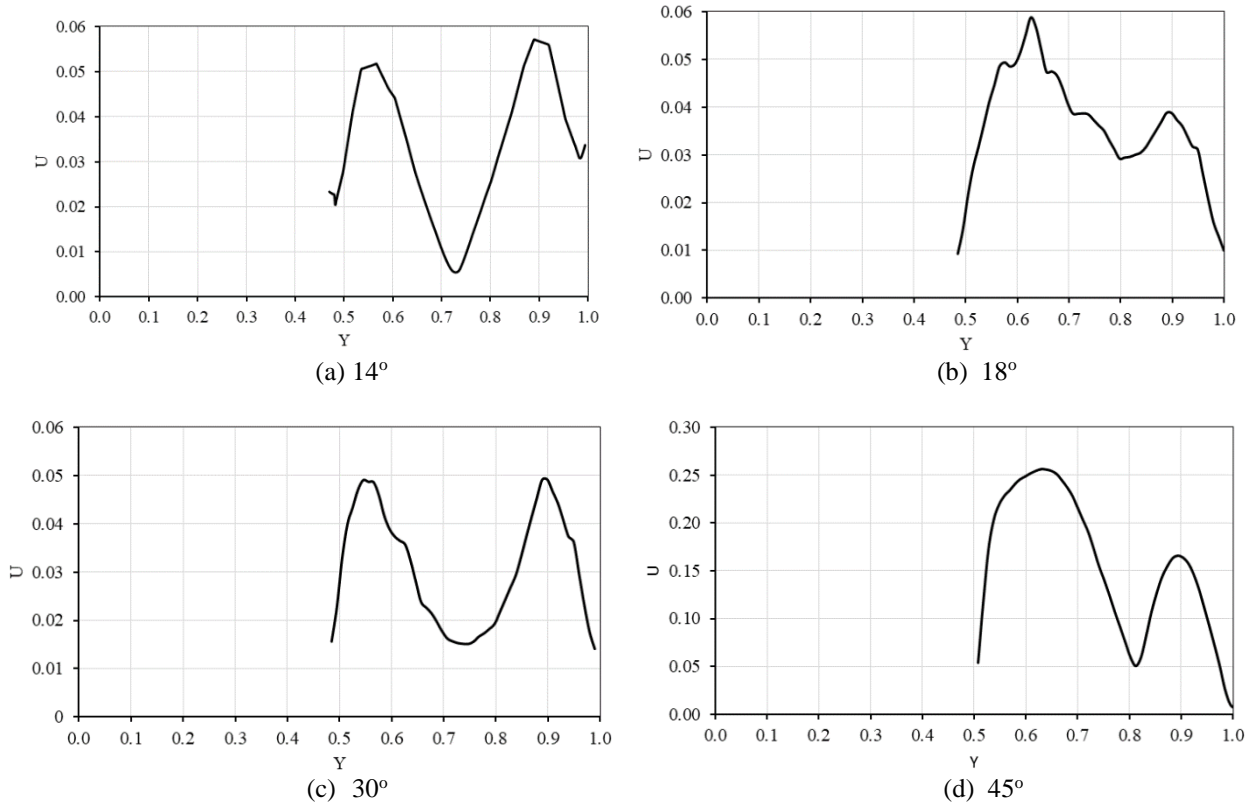
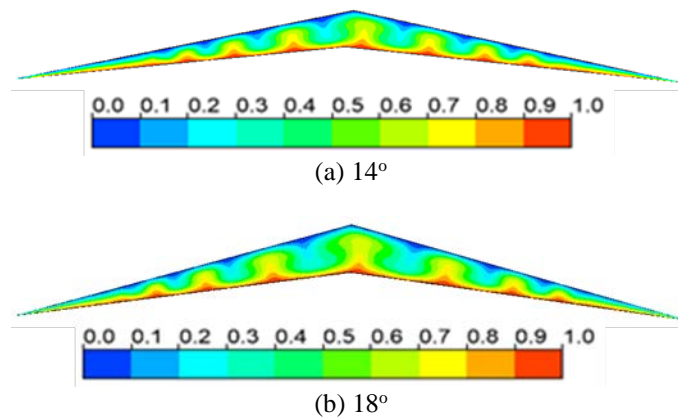


Figure 6: Air velocity across midlength ($X = 0.5L$) for different enclosures

In many cases, to vent the attic, attention is often paid to the midsection. Therefore, the values of the air velocity across the vertical centreline ($X = 0.5L$) for different enclosures are indicated in Figure 6. In some of the enclosures, the cross-section forms a chord on the cell at the midsection. But, in the 45° enclosure, it coincides with the central plume. Hot air, propelled by buoyant force, accelerates upwards to a maximum velocity and thereafter losing its strength as it moves towards the cold upper wall. The peaks connote locations with high velocities while the troughs fall within the core area of a cell. The plot along this vertical cross-section enables the velocity at a point at the midsection of any enclosure to be predictable.

3.3 Temperature Field

Figure 7 shows the contour plots of the dimensionless temperature, θ , in form of isotherms within the enclosures. The temperature distributions characteristically show hot air in forms of plumes rising from the hot lower wall and jets of cold air flowing downward from the upper wall in a pattern similar to the sequence of the streamlines. Combination of half of a plume and half of an adjacent jet form a vortex thereby making a plume or a jet to be between two counter-rotating cells. The thorough mixing of air within the 14° enclosure makes average temperature within the attic to be highest in comparison with other roof pitches. Also, as the pitch angle increases, the volume of air to be heated increases and hence the average temperature reduces. There is no evidence of thermal diffusion in any of the enclosures.



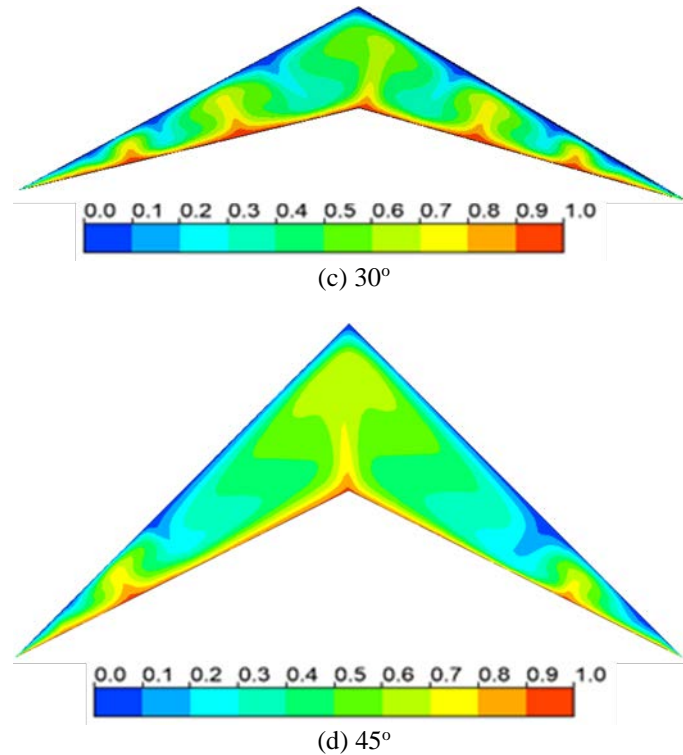


Figure 7: Temperature field for different pitch angles

Figure 8 shows together the variation of the dimensionless temperature at a cross-section slightly above the midheight ($Y = 0.6H$) for all the enclosures. The pattern shown is synchronous with the flow field within each enclosure. The peaks correspond with the middle of the plumes while the trough falls on the middle of the cold jets. Hence, the span between a peak and an adjacent trough connotes the length of chord across a cell at a location. From the plot, it could be seen that the average dimensionless temperature along the cross-section is 0.45.

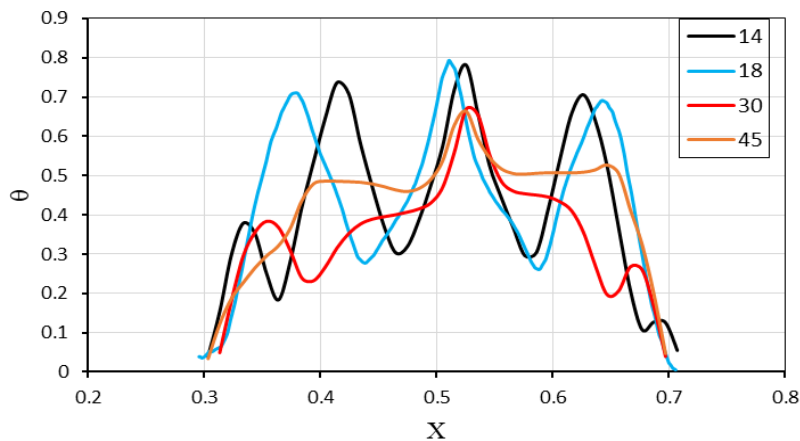


Figure 8: Air temperature across $Y = 0.6H$ for different enclosures

Being a region of importance, attempt was made to know the variation of air temperature at the vertical centreline ($X=0.5L$) for all the enclosures is shown in Figure 9. For most of the enclosures, the plots show that temperature reduces gradually as the hot air in the central plume rises upward into colder volume of air, stabilizes at about the midheight and decreases steadily in the upper boundary layer within which there is high temperature gradient.

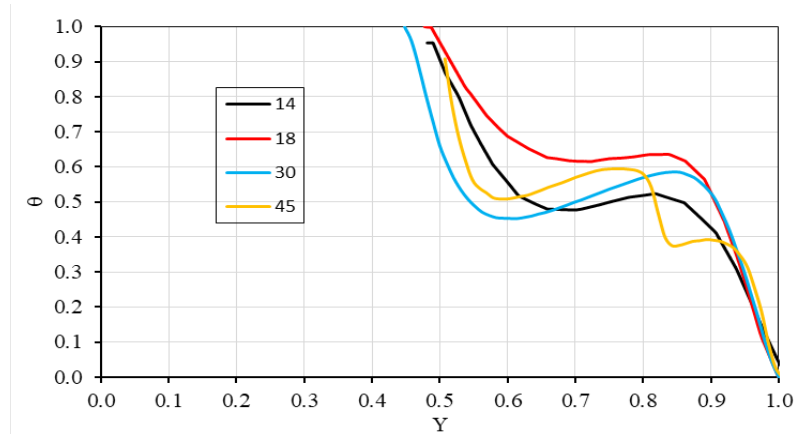


Figure 9: Air temperature at midlength ($X = 0.5L$) for different enclosures.

The profiles of the dimensionless temperature similar to those shown in midlength, at the midheight and other cross-sections within enclosures of the same configuration could be used to predict the actual thermal condition at any point in the attic.

3.4 Heat Transfer

The Nusselt number variation along the walls is mostly used to illustrate the rate of heat transfer from a surface. In Figure 10, the local Nu plot for the hot lower wall for the 45° enclosure is presented.

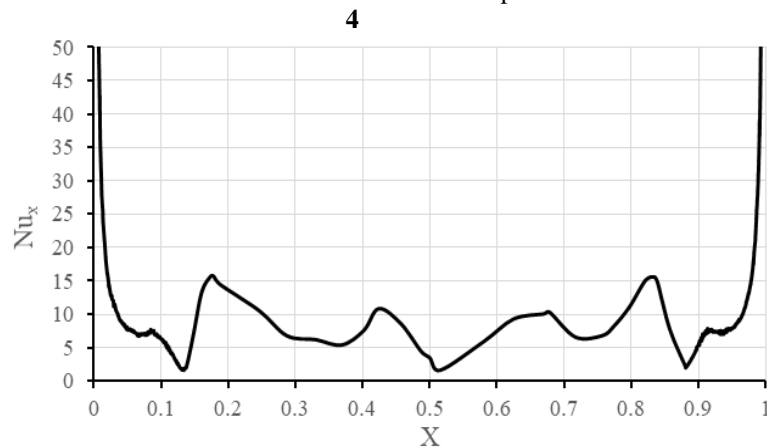


Figure 10: Local Nu plot for the hot lower wall of the 45° enclosure

The pattern of the variation synchronizes with the detachment of the hot plumes and the attachment of the cold jets from and to the hot lower wall respectively. High thermal gradients that occur at locations where cold jets drop on the hot lower wall results in peak values of the Nu_x . The heat transfer rate is low at points where hot air separates from the hot wall thereby creating regions of near-zero temperature gradient.

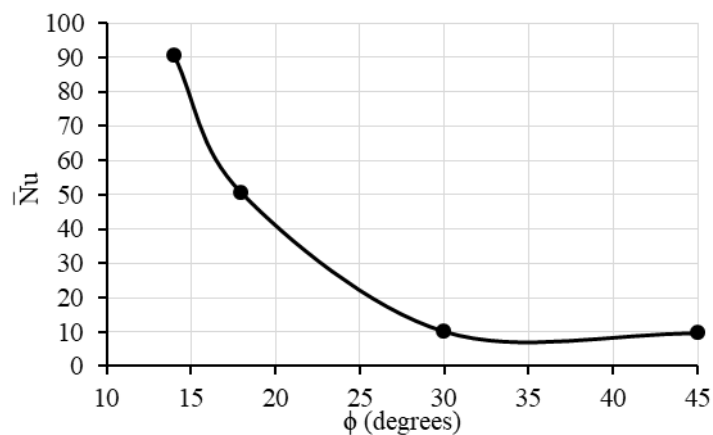


Figure 11: Mean Nusselt number of the hot base wall against pitch angle

In order to determine the average rate of heat transfer across the ceiling of a building, represented by the lower wall, the correlation between the mean Nusselt numbers of the hot wall with the enclosure pitch angle is presented in Figure 11. The plot is found to be negative-gradient. On the hot wall of the 45° enclosure, the rate of heat transfer drops considerably such that it is just 10.5% of that for the 14° roof pitch. For regular triangular attic space heated from below, Haese and Tuebner [23] reported similar rate of reduction of mean Nusselt number as the pitch angle increases. Practically, the Figure 11 shows that, in temperate environment, to minimize the rate of heat loss from the heated occupied below space into the attic above through the ceiling, the pitch angle of the roof should be relatively high. For low-pitch roof buildings, the ceiling insulation should be of appropriate quality and thickness.

4. CONCLUSION

Steady-state, two-dimensional laminar natural convection heat transfer of air in long, scissors-shaped attic of selected pitch angles heated through the ceiling has been reported. The streamlines portrays multiple, recirculating, counter-rotating cells symmetrically positioned within the enclosures. The intensity and size of the vortices decrease from the middle of an enclosure towards the bottom corners and as the enclosure pitch increases. Heat transfer rate is high at locations where cold jets drop on the hot wall but low where hot air separates from the hot wall. The pattern of the variation of the local Nusselt number along the hot wall synchronizes with the detachment of the hot plumes and the attachment of the cold jets from and to the hot lower wall respectively. The mean Nusselt number for the hot ceiling decreases with the pitch angle. The practical application of the results is that, in temperate climate, the rate of heat loss from a heated space into the attic through the ceiling could be minimized when the pitch angle of the roof is relatively high. For low-pitch roof buildings, the ceiling insulation should be of appropriate quality and thickness. Also, knowledge of the airflow patterns in the attic space could serve as a guide to rooftop designers and building users.

REFERENCES

- [1] Flack, R. D. (1980). The Experimental Measurement of Natural Convection Heat Transfer in Triangular Enclosures Heated or Cooled from Below, *J. Heat Transfer*, 102, 770-772.
- [2] Akinsete, V.A. & Coleman, T.A. (1982). Heat Transfer by Steady Laminar Free Convection in Triangular Enclosures, *IJHMT*, 25(7), 991-998.
- [3] Kamiyo, O. M., Angeli, D., Barozzi, G.S., Collins, M.W., Olunloyo, V.O.S. & Talabi, S.O. (2010). A Comprehensive Review of Natural Convection in Triangular Enclosures, *AMR: Trans. ASME*, 63(060801), 13 pages.
- [4] Das, D., Roy, M. & Basak, T. (2017). Studies on Natural Convection within Enclosures of Various (Non-square) Shapes - A Review, *IJHMT*, 126, 356-406.
- [5] Moftakhari, A., Aghanajafi, C. & Ghazvin, A.M.C. (2017). A Novel Numerical Approach for Convective and Radiative Heat Transfer Analysis of Fluid Flow Problem within Triangular Cavities using Natural Element Method, *J. Heat Transfer*, 139 (8), 082002 (13 pages).
- [6] Basak, T., Anandalakshmi, R. & Biswal, P. (2013). Analysis of Convective Heat Flow Visualization within Porous Right-angled Triangular Enclosures with a Concave/Convex Hypotenuse, *Num. Heat Transfer: A*, 64 (8), 621-647.
- [7] Haghghi, A.P., Golshaahi, S.S. & Abdinejad, M. (2015). A study of vaulted roof assisted evaporative cooling channel for natural cooling of 1-floor buildings: in *Proceedings of Sustainable Cities & Society*, 2015, paper 14, 89-98.
- [8] Zhao, D., Aili, A., Yin, X., Tan, G. & Yang, R. (2019). Roof-integrated Radiative Air-cooling System, *Energy & Buildings*, 203, 109453, 9 pages.
- [9] Das, S. & Morsi, Y. (2002). Natural Convection Inside Dome-shaped Enclosures, *IJNMHFF*, 12(2), 126-141.
- [10] Mahmoudi, A., Mejri, I., Abbassi, M.A. & Omri, A. (2013). Numerical Study of Natural Convection in an Inclined Triangular Cavity for Different Thermal Boundary Conditions: Application of the Lattice Boltzmann Method, *Fluid Dyn Mat Proc*, 9, 353-388.
- [11] Kamiyo, O.M., Angeli, D., Barozzi, G.S. & Collins, M.W. (2014). Natural Convection in Asymmetric Triangular Enclosures Heated from Below, *J. Physics*, 547, 1-10.
- [12] Saha, S.C. & Gu, Y.T. (2015). Natural Convection in a Triangular Enclosure Heated from Below and Non-uniformly Cooled from Top, *IJHMT*, 80, 529-538.
- [13] Sieres, J., Campo A. & Martinez-Suarez, J.A. (2016). Natural Convection Air Flow in Vertical Upright -angled Triangular Cavities under Realistic Thermal Boundary Conditions, *Thermal Science*, 20(5), 1407-1420.
- [14] Amrani, A., Dihmani, N., Amraoui, S. & Mezrhab, A. (2017). Analysis of Combined Natural Convection and Thermal Radiation Heat Transfer in a Triangular-shaped Roof for Hot Climates, *Mater. Envir. Sci.*, 8(8), 3013-3027.

- [15] Cui, H., Xu, F., Sahad, S. & Liu, Q. (2019). Transient Free Convection Heat Transfer in a Section Triangular Prismatic Enclosure with Different Aspect Ratios, *Int. J. Thermal Sciences*, 139, 282-291.
- [16] Elnokaly, A., Ayoub, M. & Elseragy, A. (2019). Parametric Investigation of Traditional Vaulted Roofs in Hot-Arid Climates, *Renewable Energy*, 138, 250-262.
- [17] Mehryan, S.M., Mohammad, G., Reza, K.F., Ahmad, H. & Mohsen, I. (2020). Free Convection in a Trapezoidal Enclosure Divided by a Flexible Partition, *IJHMT*, 149, 119186, 14 pages.
- [18] Kamiyo, O. (2020). Numerical Simulations of Natural Convection for Raised-ceiling Rooftop Heated from Below, *KJE*, 11 (4), 58-71.
- [19] Penot, F. & N'Dame, A. (1992). Successive bifurcations of natural convection in a vertical enclosure heated from the side, Heat Transfer: in *Proceedings of 3rd UK NCFECTS*, 1992, 507-513.
- [20] Gray, D.D. & Giorgini, A. (1976). The Validity of the Boussinesq Approximation for Liquids and Gases, *IJHMT*, 19, 545-551.
- [21] Ridouane, E. H., Campo, A. & McGarry, M. (2005). Numerical Computation of Buoyant Airflows Confined to Attic Spaces under Opposing Hot and Cold Wall Conditions, *Int. J. Thermal Sciences*, 44, 944-952.
- [22] Holtzman, G.A., Hill, R.W. & Ball, K.S. (2000). Laminar Natural Convection in Isosceles Triangular Enclosures Heated from Below and Symmetrically Cooled from Above, *J. Heat Transfer*, 122(3), 485-491.
- [23] Haese, P.M. & Teubner, M.D. (2002). Heat Exchange in an Attic Space, *IJHMT*, 45, 4925-4936.